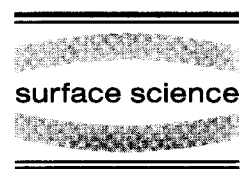




ELSEVIER

Surface Science 366 (1996) 531–544



# Surface colloid evolution during low-energy electron irradiation of $\text{CaF}_2(111)$

M. Reichling<sup>a,\*</sup>, R.M. Wilson<sup>a,b</sup>, R. Bennewitz<sup>a</sup>, R.T. Williams<sup>b</sup>, S. Gogoll<sup>a</sup>,  
E. Stenzel<sup>a</sup>, E. Matthias<sup>a</sup>

<sup>a</sup> *Fachbereich Physik, Freie Universität Berlin, Arnimallee 14, 14195 Berlin, Germany*

<sup>b</sup> *Department of Physics, Wake Forest University, Winston-Salem, NC 27109, USA*

Received 29 February 1996; accepted for publication 30 May 1996

## Abstract

The effects of 1 keV electron irradiation (current density typically  $40 \mu\text{A cm}^{-2}$ ) on the surface structure of  $\text{CaF}_2(111)$  are studied by scanning force microscopy (SFM) to investigate the role of diffusion in the process of electron-induced surface metal colloid formation. Systematic variation of beam voltage, irradiation time, intensity and dosage is investigated in regard to metal formation on  $\text{CaF}_2$  surfaces. The main features observed in an experiment with constant irradiation intensity are colloids on the surface growing from an average size of 50 nm at a dosage density of  $0.66 \text{ mC cm}^{-2}$  to 200 nm at  $85 \text{ mC cm}^{-2}$ . The surface metal volume first increases quadratically in time and saturates at dosage densities above  $6 \text{ mC cm}^{-2}$  due to the increasing coverage of the surface by metal. Such a quadratic dependence confirms that surface metal is created by electron-stimulated F-center diffusion from the bulk. By varying current density we also find a saturation in F-centers arriving at the surface. A competing mechanism of metal creation directly at the surface becomes dominant for current densities above  $50 \mu\text{A cm}^{-2}$ . In this intensity regime we find dosage-dependent metallization features showing a transition from metallic clusters of 30 nm diameter to larger aggregates and formation of  $\mu\text{m}$ -sized blisters with increasing dosage. For highest irradiation dosages, the main features are large irregularly shaped metal platelets with folded ridges of approximately 150 nm elevation. We propose that these result from the collapse of blisters that were previously filled with fluorine gas resulting from the radiolysis of the halide crystal. Furthermore, the  $\text{CaF}_2$  surface is investigated after removal of the metallic deposits by water treatment. SFM images reveal the existence of holes about 30 nm in diameter, which grow into a random network of larger grooves at higher dosages.

**Keywords:** Atomic force microscopy; Calcium difluoride; Clusters; Diffusion and migration; Electron bombardment; Radiation damage; Stepped single crystal surfaces

## 1. Introduction

Among the alkaline-earth halides,  $\text{CaF}_2$  is notable as a deep-UV window material [1], thin film optical coating [2,3], and as an insulating film which can be epitaxially grown on semiconductor

surfaces [4–9]. The morphology of such films has been characterized by SEM, LEED and SFM [10,11]. Surface modification of  $\text{CaF}_2$  films by photon [12,13] and electron [14–16] irradiation has been studied. It is of interest for the possibility of high-resolution patterning of  $\text{CaF}_2$  crystals and films by photons [17] and electron beams [18–21]. The ultimate goal of such studies is patterning techniques that are capable of creating

\* Corresponding author. Fax: +49 30 8386059;  
e-mail: reichling@matth1.physik.fu-berlin.de

structures of less than 2 nm in size [22] for the fabrication of insulating microstructures on semiconductors.

Despite several decades of investigation into the problem of colloid growth in the bulk [23] of alkaline-earth halides by optical spectroscopy [24–26] and transmission electron microscopy [27,28], the structure and spatial distribution of surface colloids is not well understood. The use of scanning force microscopy can be particularly helpful in such studies since it allows accurate topographic imaging of the development of metallic clusters and pits on electrically insulating surfaces [29,30], and has the potential of being extendable to the atomic level [31,32].

CaF<sub>2</sub> is a particularly interesting material for studying colloid formation and surface metallization, since the lattice constant of calcium metal (5.565 Å, fcc) and the Ca<sup>2+</sup> sublattice in the fluorite crystal (5.451 Å, fcc) match closely [28], making colloid formation unusually efficient. Electron-beam excitation of CaF<sub>2</sub> results primarily in valence electron–hole pairs, which form self-trapped excitons (STEs) with very high efficiency. Some of the STEs separate into defect pairs of an F center and interstitial fluorine [33]. Optical extinction spectra observed following electron irradiation at temperatures between room temperature and 450 K exhibit a strong bulk colloid absorption band, while the F-center absorption is relatively weak [34], indicating that aggregation of F centers

to form metal colloids is the favored stabilization channel.

In the present paper we discuss the main features of surface colloid formation on CaF<sub>2</sub> (111) irradiated by low-energy electrons (about 1 keV). This includes their development as a function of electron energy, current, irradiation time and total dosage. For a systematic study five series of measurements have been performed with experimental parameters compiled in Table 1. In each series, one parameter was varied systematically while the others were kept constant. The electron energy was kept constant at 1 keV except for series IV, where we studied the dependence of the metallization on electron energy. Series I was designed to follow the amount of metal appearing at the surface as a function of dosage from the first effects detectable on a nm-scale to later stages, where most of the surface is covered by metal. To investigate the effect of irradiation time independent of dosage, we varied irradiation time and current density in series II while preserving a fixed dosage for the complete series. Series III complements the constant dosage experiment by isolating the effect of current density independent of time. To study the influence of electron penetration depth, in series IV the electron energy was varied over the range accessible to our electron source. In the final series (V) we studied high current-density effects by taking SFM images across a Gaussian irradiation profile of a heavily irradiated spot.

Table 1

Compilation of irradiation data; SFM measurements have been designed for a systematic variation of one experimental parameter in each series; series I was a study of the metallization as a function of irradiation time  $t$  at constant current density; in series II irradiation time  $t$  and current density  $j$  were varied to obtain spots subjects to identical dosage densities; in series III the irradiation time was kept constant while the current density  $j$  was varied; series IV represents images taken at four different electron energies  $E$ ; series V is similar to III, however, different current densities were measured across an electron beam profile and the maximum applied current density was the highest of all measurements

Series	I	II	III	IV	V
Parameter variation	$\Delta t$	$\Delta(j, t)$	$\Delta j$	$\Delta E$	$\Delta j$ (prof.)
Sample temperature $T$ (K)	420	410	440	440	450
Electron energy $E$ (eV)	1000	1000	1000	500–2000	900
Irradiation time $t$ (s)	20–2560	20–80	40	40	58
Current density $j$ ( $\mu\text{A cm}^{-2}$ )	33	17–70	17–70	42	10–100
Dosage density $jt$ ( $\text{mC cm}^{-2}$ )	0.66–85	1.4	0.68–2.8	1.7	0.58–5.8
Results shown in	Fig. 5	Fig. 7	—	Fig. 9	Fig. 11

It is known [35] that the rate of metallization of irradiated  $\text{CaF}_2$  increases with temperature. For measurements of series I and II we kept the crystal at temperatures of 420 and 410 K, respectively, to limit the rate of metal coverage and saturation effects. The other experiments were performed at temperatures of 440 and 450 K, with a notably higher metallization efficiency.

## 2. Experiment

### 2.1. Irradiation conditions

Measurements were performed on commercial UV-grade synthetic  $\text{CaF}_2$  single crystals ( $20 \text{ mm} \times 20 \text{ mm}$ ) grown by Karl Korth. The crystals were cleaved in air along a (111)-plane and transferred into the UHV chamber ( $p < 10^{-9}$  mbar) within 15 min after cleavage. Cleaved crystals were cleaned by heating to 700 K in UHV. By XPS, we have observed that after 200 min at 600 K, oxygen and carbon contaminants were reduced to 25 and 50% of the initial values, respectively. While the trend in the oxygen data indicated that a further reduction would have been possible by prolonged heating, the carbon signal approached a constant value after 100 min of heating.

For the irradiations we used an electron source providing 0.5–2 keV electrons at currents from 1 to 10  $\mu\text{A}$ . The electron beam intensity profile was monitored with a CCD camera observing the STE luminescence from the irradiated sample. Electrons were either focused into a spot of approximately  $0.8 \text{ mm}^2$  in area at the sample surface for high intensity irradiation (series V), or defocussed to a spot size of  $12 \text{ mm}^2$  for low current densities (series I–IV). In series V, the spot was defined by the  $1/e^2$  diameter of the Gaussian intensity distribution, while in the other series we obtained a nearly top-hat beam profile. In all cases, SFM measurements were performed in the center of the irradiated spots where there was a well defined beam intensity ranging from 17 to 70  $\mu\text{A cm}^{-2}$ . For the high-intensity measurement (series V) the sample was irradiated with a center intensity of 100  $\mu\text{A cm}^{-2}$  for 58 s. In this way an irradiated spot was

prepared which received a maximum dosage of 5.8  $\text{mC cm}^{-2}$  in its center.

### 2.2. Force microscopy

Scanning force microscopy was performed in air on selected areas of the irradiated spots after removal from the vacuum chamber. That is, in this work we are studying oxidized records of the location, size and shape of calcium colloids or islands that were formed under irradiation in UHV. It is a crucial assumption for this method that there should not be large-scale mass motion on the surface as a result of exposure to air at room temperature. We believe that this assumption is rather well supported in regard to surface features in the size range  $> 10 \text{ nm}$  by the following observations. Progressive changes of the topography observed in dry air at room temperature have not been found over a period of weeks. One of the best arguments for stability of metallization features after electron irradiation in vacuum even at 400 K is the fact that progressive development or motion of the metal colloids has been found to be almost exclusively limited to the time that the electron beam is switched on. Using optical methods that are very sensitive to small changes in size and shape of colloids, changes could only be observed a few minutes after turning off the electron irradiation and then the optical response was stable for hours of observation time [36]. Colloids prepared at 150 K rapidly grow in size by a ripening process when warmed to room temperature. However, further heating to 400 K produces only minimal alteration of colloid radii [36]. If thermal diffusion is negligible for several hours at 400 K, then we expect no changes in topography during extended storage or handling at 300 K. To further investigate the influence of air exposure, some of the observations reported here have been repeated with an SFM mounted in a UHV chamber, so that there is no air exposure between irradiation and observation. Then, air was admitted and the measurement repeated in air on the same spot. It was found that the air exposure does not induce any significant change in the images. Details of this experiment are discussed below. SFM images were reproducible and no tip-induced erosion was found on the

time scale of our observations, as long as the tip force was kept less than 100 nN. When applying forces above 160 nN, evidence for material removal was detected.

The analysis of images included the determination of the amount of metal left on the surface after electron irradiation. This was done using in-house software to determine the  $\text{CaF}_2$  surface level in the SFM images and to integrate over all features above the surface plane. Care was taken to avoid erroneous results from step edges or image distortions. Since the observed metal features are mostly flat and large compared to the tip curvature, results are not expected to be influenced by geometry-related artifacts. Colloid volumes obtained in this way are presented as an equivalent uniform metal-layer thickness. Due to the match in lattice constants, the equivalent metal thickness is comparable to the thickness of the removed  $\text{CaF}_2$  layer. Thus, we are able to obtain absolute numbers for the  $\text{CaF}_2$  sputtering efficiency under various sputtering conditions.

Fig. 1 shows a typical unirradiated  $\text{CaF}_2$  surface. The surface is essentially flat and the only features observable on a scale typically used for measurements presented here are step edges resulting from cleavage of the crystal. Their size generally ranges from monoatomic steps to macroscopic edges clearly visible by eye. Step edges were generally aligned along the natural (111) cleavage directions of the  $\text{CaF}_2$  crystal. However, we also found steps making an angle of  $15^\circ$  with respect to the (111) directions, as have been reported by other authors [37].

To clarify the influence of surface steps on electron-induced colloid formation, a variety of images were taken under different experimental conditions. Colloids produced under typical conditions ( $20 \mu\text{A cm}^{-2}$  for 80 s) are shown in Fig. 2. This illustrates a general observation that colloid formation occurs with equal probability on terraces and close to cleavage steps. Most measurements did not show any evidence for an enhanced, diminished or qualitatively changed formation of colloids at step edges. Occasionally, under specific conditions of very high dosages and temperatures, step edges were observed to act as barriers against

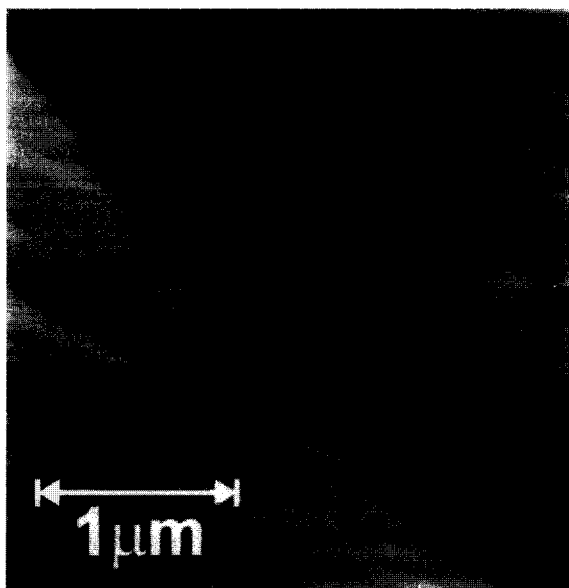


Fig. 1. SFM image of the unirradiated  $\text{CaF}_2$  (111) surface. The main features are cleavage steps with a height ranging from a F–Ca–F triple layer to macroscopic dimensions. Macroscopic steps are normally not aligned along a crystallographic direction but are determined by the stress during cleavage. For small steps the predominant direction is the (111) direction. Angles between steps reproduce the inclination of higher index crystallographic planes with respect to the (111) plane.

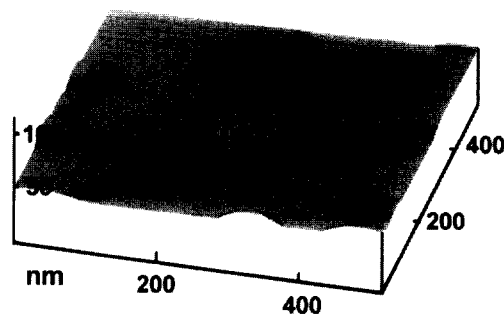


Fig. 2. SFM image of Ca colloids on the  $\text{CaF}_2$ (111) surface. The surface was irradiated for 80 s under conditions similar to those of series I described in Table 1. Colloids appear in the form of flat precipitates randomly distributed over the surface.

surface diffusion, and metal collected along the edge.

To verify that the surface colloid morphology and metal volume determined by imaging in air represent those in vacuum, we produced surface

colloids of a height lower than 25 nm and a lateral extension of some hundred nm. A  $4\ \mu\text{m} \times 4\ \mu\text{m}$  region of the prepared surface was imaged in UHV and again 10 min later after exposure of the surface to the ambient atmosphere. Results of this comparative study are shown in Fig. 3. Imaging in UHV turned out to be much more difficult than similar studies in air. Images are quite often distorted by stripes originating from colloids as seen for example, in the upper part of the UHV image in Fig. 3. Since the lower part had been scanned before, we speculate that the stripes are a result of electron-irradiation related charging of the surface that is in part still present even after exposure to air. This phenomenon probably also explains the somewhat softer appearance of colloids in the UHV image compared to the air image. A more detailed analysis of UHV imaging features will be reported in future publications. The main result for the present

work, however, is that despite the described artifacts both images are virtually identical, not only by the visual impression but also with respect to a quantitative analysis. This is demonstrated by the cross-sections shown in Fig. 3, taken along the same line in both images. The cross-sections differ only by some subtleties caused by scanning artifacts, but the lateral extension and the height of the features coincide within an error of only a few per cent. Since this is not a single result but the general observation in many parts of the surface, we conclude that colloid morphology and metal volumes determined in air are identical to those prepared in vacuum.

### 2.3. Colloid oxidation in UHV

The formation of an oxide layer during electron-stimulated decomposition of  $\text{CaF}_2$  thin films under

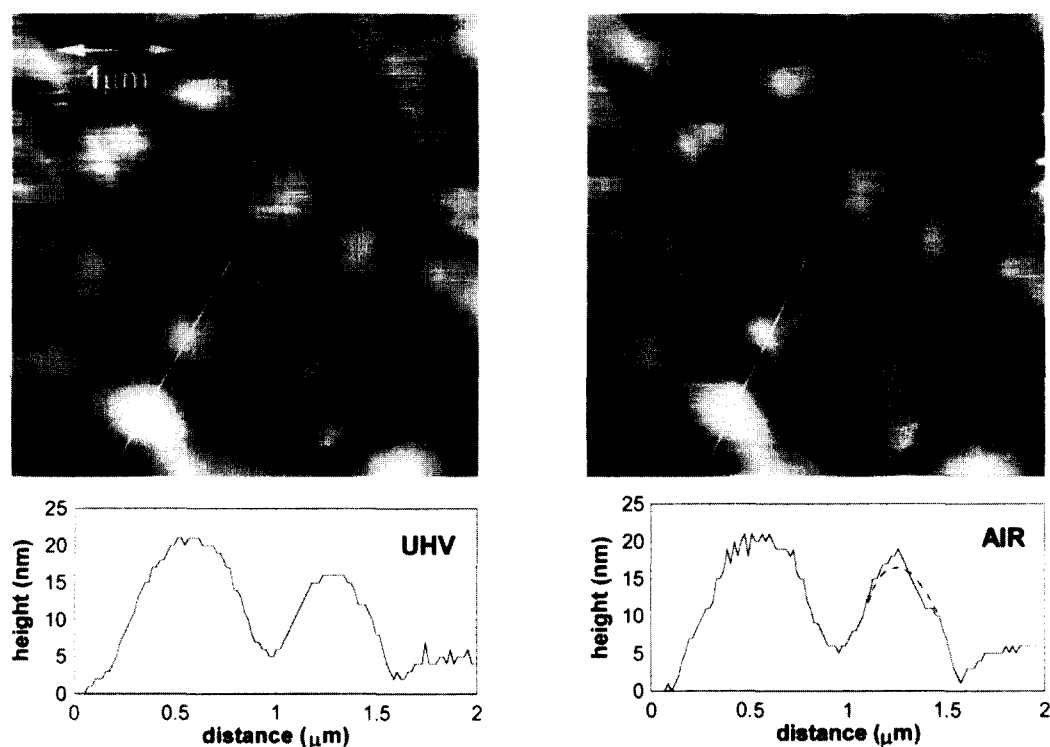


Fig. 3. Comparative study of colloids on  $\text{CaF}_2$  (111) observed in UHV and air. The figures represent the same surface region before and after exposure to the ambient atmosphere. Height profiles were taken along the white lines in the SFM images. The dashed line in the air profile symbolizes the true profile and is drawn to demonstrate that scanning artifacts may lead to a distortion of profiles but often do not influence the volume determination, since positive and negative deviations cancel each other.

UHV conditions has been demonstrated by several authors [38,39]. With XPS we investigated the question of in-situ oxidation of metal colloids during their formation under conditions used for our SFM measurements. XPS measurements of the Ca 2P doublet and O 1 s line were performed on the unirradiated and irradiated surface. On the unirradiated surface no oxygen could be detected within the precision of our measurement, and the Ca lines appeared at their regular positions expected for the CaF<sub>2</sub> crystal. During irradiation at a base pressure of  $2 \times 10^{-10}$  mbar a shoulder developed on the high-energy side of the doublet, as shown in Fig. 4a. We interpret this new line as the chemically shifted Ca line from oxidized metal. This interpretation is supported by the simulta-

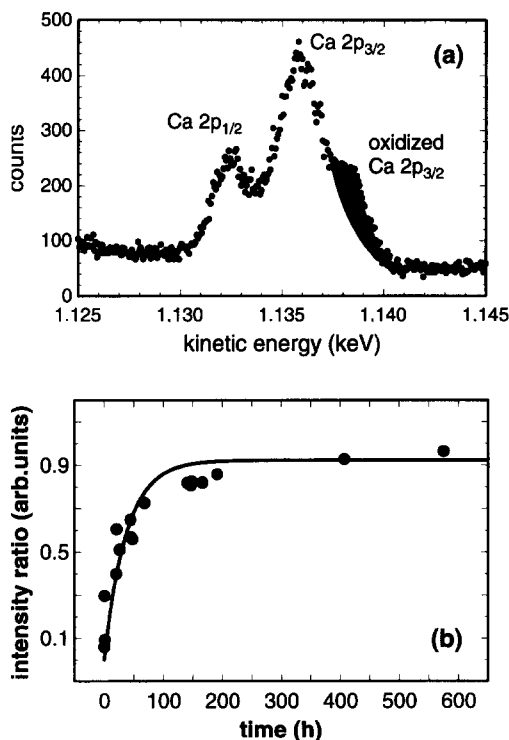


Fig. 4. XPS observation of Ca oxidation on the electron irradiated CaF<sub>2</sub> surface. (a) The shaded area results from a chemical shift of the Ca 2p<sub>3/2</sub> line due to oxidation and is not present on a clean crystal. (b) Temporal development of the O 1s/Ca 2p line intensity ratio as a function of time after irradiation. The sample had been irradiated with  $7 \text{ mC cm}^{-2}$  of 4 keV electrons at 200°C. The solid line represents a fitted exponential with a rise time of 38 h.

neous appearance of the O 1 s signal. Fig. 4b shows the temporal development of the intensity ratio between the oxygen and calcium signals after irradiation for a time which is short compared to the time of the following observation. Immediately after switching off the electron current, oxidation starts and the oxygen signal rises rapidly. Later the accumulation rate becomes smaller and the signal starts to saturate about 200 h after irradiation. An estimate of the time evolution of the formation of one monolayer of oxide during exposure to the residual gas yields an exponential oxide growth with a time constant of about 100 h, which is compatible with the development observed in Fig. 4b. Within this model, oxidation has reached 0.04% of a monolayer for a typical exposure time of 50 s at a pressure of  $2 \times 10^{-10}$  mbar. Therefore, it must be concluded that oxidation certainly appears during colloid formation even in UHV, and may affect the formation of surface chemical structure and topography when the irradiation time exceeds a few minutes.

### 3. Low-intensity irradiation

#### 3.1. Constant irradiation current, varying irradiation time

For series I, 6 spots of the CaF<sub>2</sub> surface were irradiated at a temperature of 420 K with 1 keV electrons at  $33 \mu\text{A cm}^{-2}$  for increasing periods of time. The resulting series of images is shown in Fig. 5. Qualitatively, the number of surface colloids is already large after 40 s, and with increasing time of irradiation, the islands grow larger and coalesce. One parameter that can be compared to models of surface metallization is the total volume of surface colloids. This is plotted as filled circles in Fig. 6 as a function of irradiation time. Using data from Fig. 5a for the irradiation with the lowest total dose, we find that about 90 electrons (i.e. 2500 primary excitations) are required to create one surface Ca atom. For the longest irradiation time where no saturation occurs (160 s), the efficiency rises to 15 electrons for one surface Ca atom. From the double-logarithmic plot, it is seen

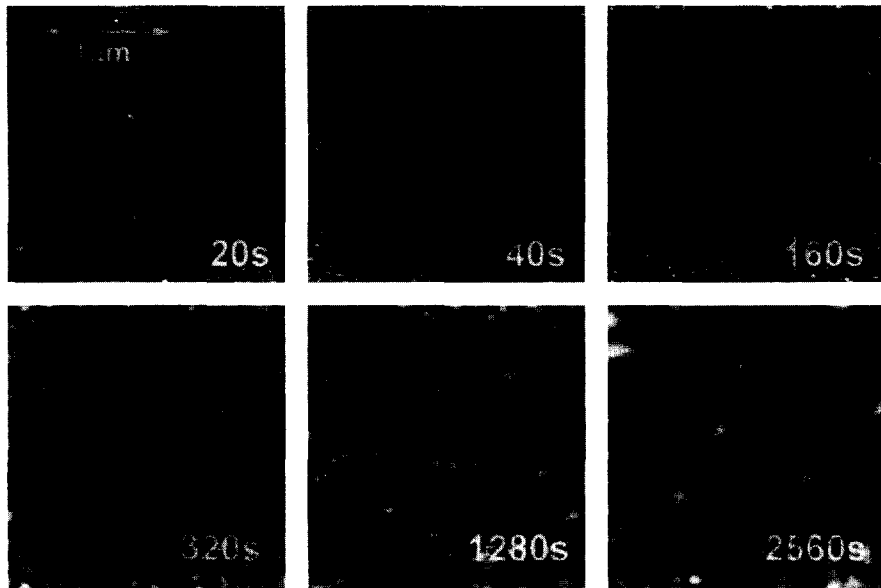


Fig. 5. SFM images from series I of irradiation at constant current density of  $33 \mu\text{A cm}^{-2}$  for increasing irradiation time.

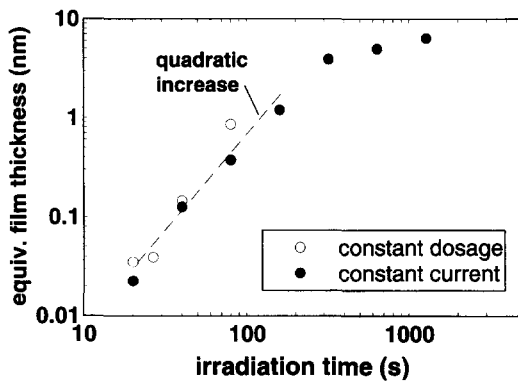


Fig. 6. Equivalent metal-layer thickness (total metal volume per  $2 \mu\text{m} \times 2 \mu\text{m}$ ) determined from SFM images as a function of irradiation time. (●): Constant current density series I (Fig. 5). (○): Constant dosage series II (Fig. 7). The dashed line indicates a quadratic increase.

that the amount of surface metal first increases quadratically with irradiation time before it saturates at higher dosages. The saturation is a result of increasing coverage by metal, which partially blocks the incoming electrons.

Note that a simple proportionality of surface metal to radiation dose would yield a curve linear in irradiation time prior to saturation. As an explanation for the initial quadratic dependence,

we consider a Jain Lidiard type model [40], applied here to surface metal formation. We assume that metallization is mainly driven by the diffusion of F centers [41] from the bulk to the surface. F H pair production and diffusion is strongly enhanced by excitation (i.e. electron irradiation), and at 400 K is effectively limited to the period of electron irradiation. This assumption will be validated by comparison of the resulting model to experiments.

It is reasonable to expect that the number of F centers within the penetration depth of the electron beam is a linear function of irradiation time prior to saturation.

$$\frac{dN_{\text{F}}}{dt} = A_0, \quad (1)$$

where  $A_0$  is constant. This is reasonable, but not necessarily obvious, because the F centers are known to condense into bulk colloids. In fact, optical transmission spectroscopy shows that the F-center absorption signal is small compared to the bulk colloid absorption at the same dose [34]. It has already been shown that under the experimental conditions of irradiation used in the present study, the amount of metal in surface colloids is

much smaller than that in bulk colloids [36]. This means that the F centers stored in the form of bulk Ca colloids are a major source of  $N_F$  in Eq. (1).

The next postulate of this model is that the rate of arrival of F centers at the surface,  $dN_S/dt$ , is proportional to  $N_F$  in the bulk irradiated layer

$$\frac{dN_S}{dt} = KN_F. \quad (2)$$

F centers reaching the surface are assumed to aggregate with formation of Ca metal. This ignores F centers created directly on the surface, but this issue and the contribution of near surface defects to colloid formation will be critically revisited in Section 4. Eq. (2) is a general statement of one-dimensional diffusion down a concentration gradient proportional to  $N_F$ . Combining Eqs. (1) and (2) gives the relation matching the observed result

$$N_S \propto t_2. \quad (3)$$

Thus the experimental results presented in Fig. 6 yield evidence that the surface metallization is driven by F-center diffusion from the bulk under conditions of low-intensity irradiation and that the diffusion is restricted to the time of electron irradiation.

### 3.2. Constant irradiation dose, varying irradiation time and current

SFM images of  $\text{CaF}_2$  irradiated with a constant dose (series II) are shown in Fig. 7. The values of surface metal volume for this series are included as open circles in Fig. 6. Surprisingly, the amount of metal on the surface increases strongly with time, even though the corresponding current was decreased as exposure time increased to maintain a constant dose. Additionally, an increase of mean colloid size with increasing irradiation time can be observed. The number density of large colloids (i.e. those with a diameter larger than 50 nm) increases with time, as shown in Fig. 8. The total volume per unit area of surface colloids, on the other hand, has approximately the same quadratic dependence of metal volume on irradiation time as in the constant current case (cf. Fig. 6), despite the fact

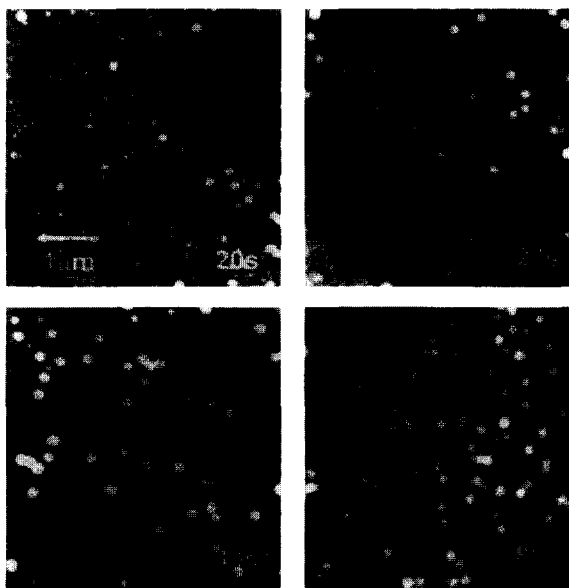


Fig. 7. SFM images from series II of irradiation at constant dosage density of  $1.4 \text{ mC cm}^{-2}$  for increasing irradiation time.

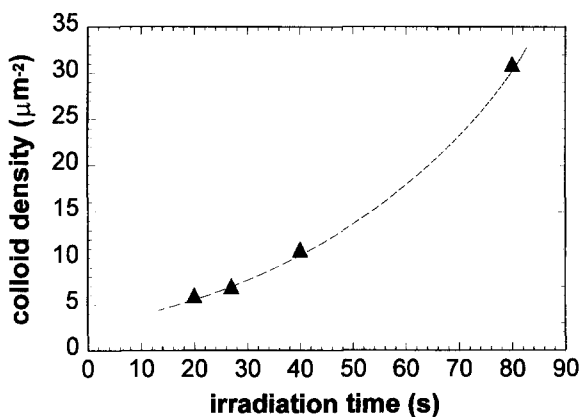


Fig. 8. Number density of large colloids ( $> 50 \text{ nm}$ ) as a function of irradiation time for series II (Fig. 7). The dashed line is a guide to the eye.

that beam current here is decreased reciprocally with exposure time. This independence of current density suggests that there is a saturation in bulk defect density, in agreement with measurements of the sputtering efficiency for different current densities [41]. Fig. 7 reveals the generation of a large number of small colloids (diameter below 50 nm) at higher irradiation intensities. In a series of measurements (series III) where the  $\text{CaF}_2$  surface

was irradiated for 40 s with current density systematically varied from 17 to  $70 \mu\text{A cm}^{-2}$ , all images had about the same number of large colloids, but there was a background of small colloids increasing in number with current density. In the previously described measurements, the amount of metal nucleating in large surface colloids was found to be approximately independent of current density. The model of Section 3.1 describes the growth of these colloids as a function of irradiation time. Since for the higher intensity irradiation the number of the small colloids is observed to increase with current density rather than with irradiation time, we suggest that there is a separate metallization mechanism at the surface which is independent of F-center production. In fact, the Knotek–Feibelman mechanism leads to  $\text{F}^+$  desorption and production of neutral calcium at the surface [41]. The metallization resulting from this process increases linearly with irradiation intensity, and no saturation is expected for the applied current densities. We assume that surface metallization from this process at first emerges as a homogeneous coverage and then forms small colloids by surface diffusion and aggregation. In contrast, colloids produced by bulk F-center diffusion can accumulate much more material and grow to a larger size with time. Section 3.3 and Section 4 present supporting evidence for this proposal.

### 3.3. Variation of electron energy

Based on the discussion so far, the question arises as to how the amount of metal that accumulates at the surface is related to the penetration depth of electrons, which can be varied by their energy. SFM images of spots irradiated with different electron energies (series IV) are given in Fig. 9. Although the amount of metal on the surface is roughly constant, there appears to be a tendency toward larger colloids at higher electron energies. This is accompanied by a decrease of the number of surface colloids, as illustrated in Fig. 10. From a recent study [42] of the electron penetration depth in  $\text{CaF}_2$  in this energy range, we have a measure for the depth of maximum F-center production and, hence of the mean diffusion path to the surface. This information is also included in

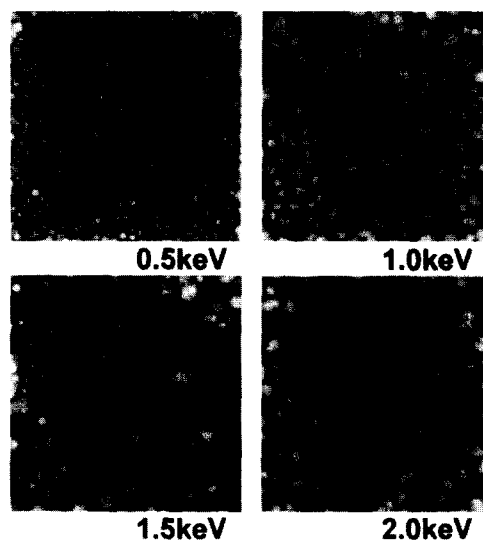


Fig. 9. SFM images from series IV of irradiation at constant current density of  $42 \mu\text{A cm}^{-2}$  and dosage density of  $1.7 \text{ mC cm}^{-2}$  for increasing beam voltage (frame size  $2 \mu\text{m} \times 2 \mu\text{m}$ ).

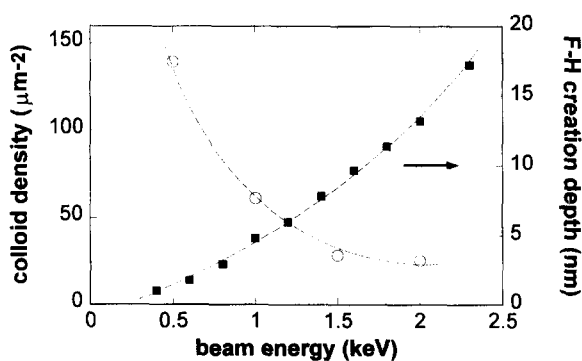


Fig. 10. (○): Colloid number density (Fig. 9) as a function of beam voltage. (■): Depth of maximum F-center production (determined from the model in Ref. [42]) as a function of beam voltage. Dashed lines are a guide to the eye.

Fig. 10, demonstrating the anti-correlation between diffusion path (F-center creation depth) and areal density of surface colloids. These results confirm the idea that metal creation close to the surface produces a large number of small colloids, while diffusion from deeper bulk enhances aggregation and results in a distribution of well-separated, larger colloids at the surface.

We attribute this observation to the fact that the F-center diffusion in reality is predominantly one-dimensional as had been assumed for simplic-

ity so far, but also significant lateral displacement may occur for defects diffusing from deeper bulk regions. We anticipate that the density of preferential nucleation sites is largest at the surface containing most structural imperfections. Therefore, F centers created on or close to the surface will instantaneously nucleate at such sites and form a variety of small precipitates before further diffusive motion could provide a chance for a collision with a larger colloid. The situation is markedly different for F centers created deeper in the bulk. During their longer diffusion path towards the surface they will necessarily experience a much stronger mean quadratic lateral deviation from their origin, and hence have a higher probability to meet larger colloids. During their diffusion, the main source of trapping will be larger colloids rather than other defects. It is well known from the theory of ripening in ionic crystals [23] that under such circumstances, a nucleation favourably occurs into larger colloids rather than into small precipitates. Therefore, a strong bulk diffusion will eventually result in a much larger mean colloid size than near surface-metal creation.

#### 4. High intensity irradiation

##### 4.1. Topography across the electron-beam profile

To investigate high-intensity irradiation effects, we used a method that differs from that described in the preceding sections. The SFM samples such a small area that one can survey a large range of different current-density exposures proceeding from the periphery to the center of the Gaussian electron-beam profile, while in each image the current density is effectively constant. By this method we assured that sample preparation, beam energy, irradiation time and temperature were constant, since all data were on one spot. Although the absolute current density is not precisely known in this case, the trend of increasing current density from periphery to center is known. One sequence (series V) of images obtained in this way for a spot subjected to a maximum dosage of approximately  $5.8 \text{ mC cm}^{-2}$  is shown in Fig. 11. Frames a–f of Fig. 11 are taken at successively decreasing dis-

tances from the center, and consequently had increasingly higher current-density exposure. An average height of the observed metal colloids was determined by image analysis for each frame, and is given in the caption to Fig. 11. In Fig. 11a, the surface damage is in the form of small (50 nm) islands where the current density was about  $10 \mu\text{A cm}^{-2}$ . Fig. 11b, at a higher current density of  $20 \mu\text{A cm}^{-2}$ , exhibits a higher density of the small islands in the background, covered by some larger (200 nm) aggregates with a more irregular shape. At higher current density exposure of  $40 \mu\text{A cm}^{-2}$  and larger viewing area in Fig. 11c, the 200 nm aggregates now form the background pattern, and superimposed are much larger ( $3 \mu\text{m}$ ) features which appear smooth on this scale to the SFM. We suggest that they were formed in vacuum as continuous films of calcium metal over some region of the surface, trapping fluorine gas formed by the electron radiolysis of  $\text{CaF}_2$ . Such features will be referred to as “blisters”. The formation of blisters is a well-studied phenomenon after intense ion bombardment of metal surfaces [43]. For the case of high-energy electron- and X-irradiation, several authors have proposed similar concepts of fluorine-gas production, based on indirect evidence like voids found in TEM images of  $\text{CaF}_2$  [27,28] or a weight loss observed during exposure of  $\text{LiF}$  to ionizing radiation [44,45]. The confining calcium skin in the present case probably has a  $\text{CaF}_2$  layer on its underside due to reaction with the fluorine, and is oxidized on its upper side. That these blisters are formed with an internal pressure is evidenced by the distinct wrinkles on the skin. The ultimate proof for the blister model would be to measure directly  $\text{F}_2$  emission when blisters collapse. However, the expected partial pressure rise from breaking blisters would barely emerge from the residual gas background level recorded by a mass spectrometer. In a typical image (Fig. 11c,  $12 \mu\text{m} \times 12 \mu\text{m}$ ) we find a total blister volume of  $0.05 \mu\text{m}^3$ , indicating a reasonable value for the total blister volume in the irradiated spot of  $1400 \mu\text{m}^3$ . Assuming atmospheric pressure inside the blisters, since many survive exposure to the atmosphere, we estimated a pressure rise of  $5 \times 10^{-11} \text{ mbar}$ . This calculation neglects the pumping rate and the likelihood that blisters do

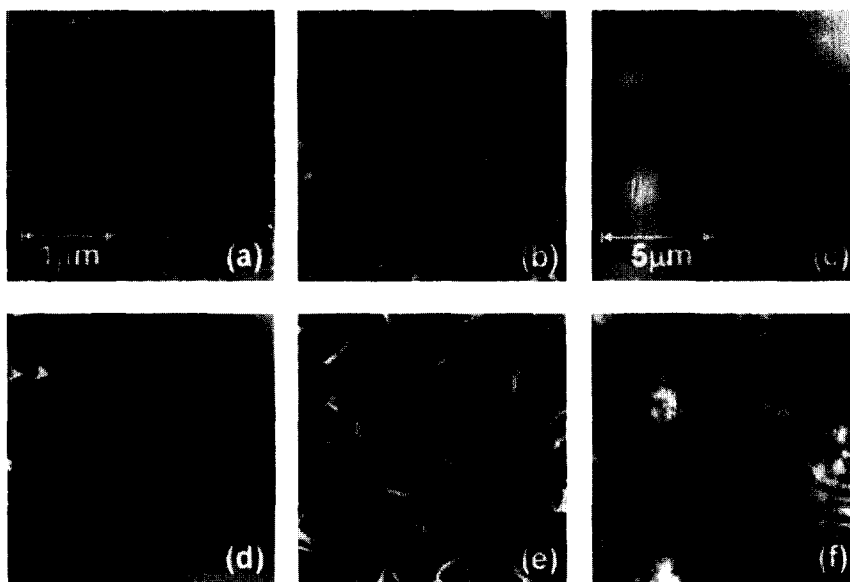


Fig. 11. Series V SFM images of the  $\text{CaF}_2$  (111) surface irradiated for 58 s with current densities of (a) 10, (b) 20, (c) 40, (d) 50, (e) 60 and (f)  $100 \mu\text{A cm}^{-2}$  (taken across the profile of a Gaussian beam). Average heights: (a) 3.6, (b) 18, (c) 38, (d) 115, (e) 145 and (f) 240 nm. Frame size: (a) and (b)  $2.5 \mu\text{m} \times 2.5 \mu\text{m}$ , (c)–(f)  $12 \mu\text{m} \times 12 \mu\text{m}$ .

not all collapse simultaneously, so this value is probably still one order of magnitude higher than the real pressure rise.

In Fig. 11d, showing the surface exposed to even higher current density, the largest blisters have grown to  $6 \mu\text{m}$ , and on the left side, some of them exhibit very distinct wrinkles, as though they are partially deflated. Fig. 11e, acquired at about half of the beam radius away from the center where the current density is  $60 \mu\text{A cm}^{-2}$ , exhibits a new kind of island structure with an intricate internal pattern of ridges suggestive of collapsed blisters. Fig. 11f was taken close to the center of the irradiation at  $100 \mu\text{A cm}^{-2}$  and indicates the transition to a new morphology of very large structures. While the aggregate on the right-hand side of this image still exhibits the ridge structure of the preceding series, the feature in the lower left corner is no longer a continuous deposit but seems to be disintegrated into smaller parts. Note that except in Fig. 11f all observed metal aggregates are rather flat, i.e. their lateral dimension is about ten times larger than their height.

From the series of images in Fig. 11 we obtained quantitative information about the metallization

efficiency as a function of current density. The effective thickness of the metallized layer is plotted against current density in Fig. 12. We conclude that metal production increases linearly with current density for the conditions of this measurement. This stands in contradiction to the model for diffusion-limited metallization at low electron intensities presented in Section 3.1, but is a natural result of our assumption that at high irradiation

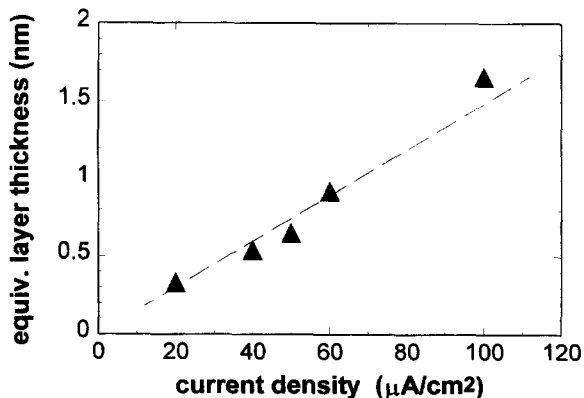


Fig. 12. Current-density dependence of equivalent surface-metal coverage determined from series V (Fig. 11).

density the dominant process for surface metallization is the creation of metal directly at the surface by the Knotek–Feibelman process.

#### 4.2. Erosion of the $\text{CaF}_2$ surface

In order to verify the water-soluble nature of the island deposits relative to the  $\text{CaF}_2$  substrate, we placed water on the irradiated sample from series V, removed the water after 1 h and dried the sample in a nitrogen atmosphere. SFM images after exposure to water are shown in Fig. 13. The lower row represents larger area scans showing a large number of cleavage steps and some deposits left even after the water treatment, while images in the upper row were taken with higher spatial resolution and reveal the detailed structure of the  $\text{CaF}_2$  surface left after exposures to 20, 60 and 100  $\text{mC cm}^{-2}$ , respectively.

The SFM images after water exposure show that the islands are completely removed, supporting our expectation that they are composed of materials like Ca, CaO, or  $\text{Ca}(\text{OH})_2$ . What is especially interesting about Fig. 13c and e are the many small pits (shown in the SFM height representation as

dark spots) left on the  $\text{CaF}_2$  surface. The size of these pits is about 30 nm, similar to the expected diameter of bulk calcium colloids [36]. Our hypothesis is that as the colloids grew and as the  $\text{CaF}_2$  surface was simultaneously eroded in favour of calcium metal and fluorine gas, the top layer of bulk colloids eventually intersected the surface, forming calcium-filled pits. Water would react with and dissolve these clusters, leaving empty pits behind.

A high degree of Ca mobility even at the late stages of surface metallization can be inferred from a comparison of Fig. 11e and f. They indicate dramatic changes in morphology, i.e. the disintegration of large area aggregates into individual droplets. Note that the average height of the calcium droplets in Fig. 11f is 240 nm, i.e. 70% larger than the height of the  $\mu\text{m}$ -diameter structures in Fig. 11e. However, the area of the newly formed droplets is roughly equal to their height. This phenomenon is attributed to a reduction in surface energy achieved by the transition of the flat metal aggregates to droplets with a shape close to the energetically most favourable spherical form. As a consequence of this process, large areas of

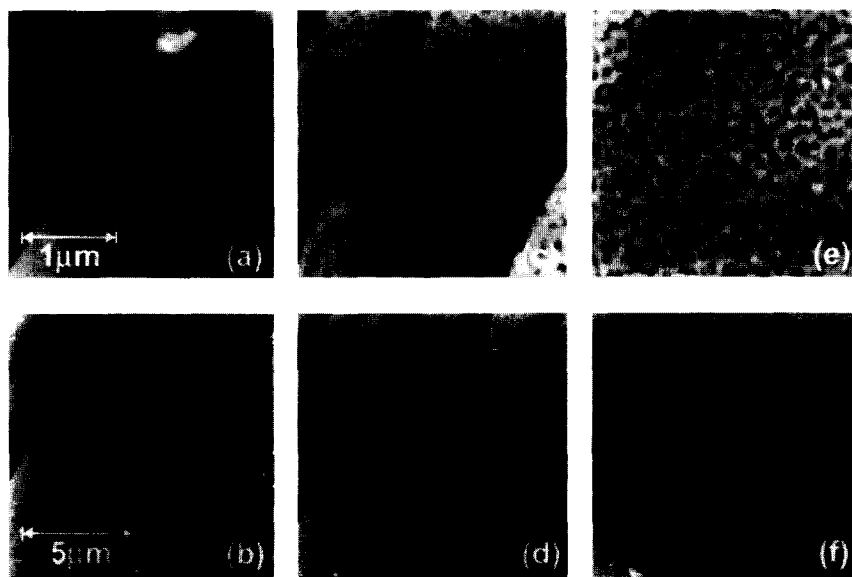


Fig. 13. SFM images of the  $\text{CaF}_2(111)$  surface electron irradiated for 58 s with current densities of (a), (b) 20, (c), (d) 60 and (e), (f) 100  $\mu\text{A cm}^{-2}$ . Surface metal has been removed by exposure to water before the images were taken. Image size is  $3\mu\text{m} \times 3\mu\text{m}$  for frames (a), (c) and (e), and  $12\mu\text{m} \times 12\mu\text{m}$  for frames (b), (d) and (f).

the  $\text{CaF}_2$  surface that had been covered by metal are exposed to electron irradiation, again giving rise to continued erosion and metallization. This should explain the observation that the metallization saturates only very slowly. The dynamical nature of surface erosion can also be inferred from a comparison of Fig. 13d and f. Surface pits are mostly well separated for the lower dosage image (Fig. 13d) but form a random network of partly connected valleys at higher dosages, as seen in Fig. 13f. We attribute this to a change of metal coverage during irradiation time, masking different areas of the  $\text{CaF}_2$  surface during the erosion process. Another interesting observation about the  $\text{CaF}_2$  erosion appears from a comparison of Figs. 13c and 13d with Figs. 13e and 13f. While the several-nm high cleavage steps are well resolved in the first two images, they can barely be recognized in the latter frames. This implies that for high-intensity irradiation such as this, erosion preferentially occurs at step edges, and we are able to remove several nm of  $\text{CaF}_2$  during electron irradiation with  $100 \mu\text{A cm}^{-2}$  for a period of 1000 s, well in accordance with measurements of the absolute amount of metal created on the surface. The metallization rate determined for  $100 \mu\text{A cm}^{-2}$  translates into an efficiency of 17 electrons needed to create one surface Ca atom. Thus the efficiency for direct surface metallization compares to that found in Section 3.1 for diffusive surface metallization for one third of the electron intensity applied for a comparable time.

## 5. Conclusions

From the results, we conclude that surface metallization by low-energy electrons occurs by two mechanisms: the creation of metal directly at the surface, and a diffusive motion of F centers from the bulk to the surface. While the surface-metal volume increases linearly with dosage for the former mechanism and is most important for high electron-current densities, the latter exhibits a quadratic dependence on irradiation time and dominates in the low-current regime. Simple modelling reveals that the quadratic increase of surface-metal volume with irradiation time is a manifestation

that F-center diffusion enhanced by electron irradiation is the rate-limiting step at low irradiation density.

For high current densities, electron-stimulated surface metallization is determined by an interplay between surface erosion due to the primary beam of electrons, surface diffusion, and the release of fluorine gas. In the initial stage, surface diffusion of F centers or fluorine vacancies leads to a formation of small colloids randomly distributed over the surface. Apparently, the nucleation of these colloids is not influenced by the large steps present on the cleaved surface. Nevertheless, we anticipate that smaller features with a size below the resolution of the images presented here – such as dislocations, point defects and small defect aggregates – could act as traps for metal migrating on the surface. Continued irradiation leads to growing colloids but also to the formation of larger-area metal films pressurized by fluorine gas emerging from the bulk. These gas-filled blisters develop to a certain size before they collapse and leave behind flat islands with a wrinkled structure. However, these structures are not inert to continued irradiation, but disintegrate and apparently convert into energetically more favourable spherical droplets. At a certain dosage level, metal colloids on most parts of the  $\text{CaF}_2$  surface inhibit F-center production in the crystal below. This masking of the surface is the limiting factor for further metallization. However, since experiments are performed at temperatures where thermal surface diffusion is not important and a complete merging of neighbouring metal structures is partly inhibited by oxide even in UHV; we never find a smooth surface Ca layer. It is a notable fact that the thickness of any complete metal layer produced by the processes described above is at least a few hundred nm and for the described experimental conditions it is not possible to produce thinner continuous films.

## Acknowledgements

The authors are grateful to T.A. Green for stimulating discussions and many valuable contributions to the work presented here. We also appreciate computer support from A. Tackett and

C. Parks during the preparation of volume calculations. This work was supported by the Deutsche Forschungsgemeinschaft, Sonderforschungsbereich 337 and by a NATO grant under contract CRG 940212. R.M.W. and R.T.W. acknowledge support from NSF grants DMR-9206745 and DMR-9510297.

## References

- [1] K. Hata, M. Watanabe and S. Watanabe, *Appl. Phys. B* 50 (1990) 55.
- [2] H.K. Pulker, *Coatings on Glass* (Elsevier, Amsterdam, 1984).
- [3] U. Kaiser, N. Kaiser, P. Weißbrodt, U. Madermann, E. Hacker and H. Müller, *Thin Solid Films* 217 (1992) 7.
- [4] M.A. Olmstead, R.I.G. Uhrberg, R.D. Bringans and R.Z. Bachrach, *Phys. Rev. B* 35 (1987) 7526.
- [5] D. Mao, K. Young, A. Kahn, R. Zanoni, J. McKinley and G. Margaritondo, *Phys. Rev. B* 39 (1989) 12735.
- [6] N. Guerfi, T.A.N. Tan, J.Y. Veuillen and R. Cinti, *Vacuum* 41 (1990) 943.
- [7] S. Sinharoy, *Thin Solid Films* 187 (1990) 231.
- [8] K.M. Colbow, T. Tiedje, D. Rogers and W. Eberhardt, *Phys. Rev. B* 43 (1991) 9672.
- [9] C.A. Lucas and D. Loretto, *Appl. Phys. Lett.* 60 (1992) 2071.
- [10] R.W. Fathauer and L.J. Schowalter, *Appl. Phys. Lett.* 45 (1984) 519.
- [11] W. Weiss, K. Kasper, K.H. Herrmann, D. Schmeisser and W. Göpel, *Surf. Sci.* 268 (1992) 319.
- [12] U.O. Karlsson, F.J. Himpfel, J.F. Morar, F.R. McFeely, D. Rieger and J.A. Yarmoff, *Phys. Rev. Lett.* 57 (1986) 1247.
- [13] W. Eberhardt, K.M. Colbow, Y. Gao, D. Rogers and T. Tiedje, *Phys. Rev. B* 46 (1992) 12388.
- [14] S. Baunack and A. Zehe, *Vacuum* 41 (1990) 1003.
- [15] K. Miura, K. Sugiura, R. Souda, T. Aizawa, C. Oshima and Y. Ishizawa, *Jpn. J. Appl. Phys.* 30 (1991) 809.
- [16] A. Izumi, K. Tsutsui and S. Furukawa, *J. Appl. Phys.* 75 (1994) 2307.
- [17] M. Oshima, S. Maeyama, H. Takenaka, Y. Ishii and H. Sugahara, *J. Vac. Sci. Technol. A* 10 (1992) 163.
- [18] T.R. Harrison, P.M. Mankiewich and A.H. Dayem, *Appl. Phys. Lett.* 41 (1982) 1102.
- [19] P.M. Mankiewich, H.G. Craighead, T.R. Harrison and A.H. Dayem, *Appl. Phys. Lett.* 44 (1984) 468.
- [20] M.A. McCord and R.F.W. Pease, *J. Vac. Sci. Technol. B* 5 (1987) 430.
- [21] Y. Hirose, S. Horng, A. Kahn, C. Wrenn and R. Pfeffer, *J. Vac. Sci. Technol. A* 10 (1992) 960.
- [22] M. Isaacson and A. Murray, *J. Vac. Sci. Technol.* 19 (1981) 1117.
- [23] A.E. Hughes and S.C. Jain, *Adv. Phys.* 28 (1979) 717.
- [24] S.D. McLaughlin and H.W. Evans, *Phys. Status Solidi* 27 (1968) 695.
- [25] V.M. Orera and R. Alcalá, *Phys. Status Solidi A* 38 (1976) 621.
- [26] V.M. Orera and E. Alcalá, *Phys. Status Solidi A* 44 (1977) 717.
- [27] L.E. Murr, *Phys. Status Solidi A* 22 (1974) 239.
- [28] E. Johnson and L.T. Chadderton, *Radiat. Eff.* 79 (1983) 183.
- [29] R.M. Wilson, W.E. Pendleton and R.T. Williams, *Radiat. Eff. Defects Solids* 128 (1994) 79.
- [30] R. Bennowitz, M. Reichling, R.M. Wilson, R.T. Williams, K. Holldack, M. Grunze and E. Matthias, *Nucl. Instrum. Methods B* 91 (1994) 623.
- [31] R.T. Williams, R.M. Wilson and H. Liu, *Nucl. Instrum. Methods B* 65 (1992) 473.
- [32] R.T. Williams, R.M. Wilson and G.P. Williams Jr., in: *Desorption Induced by Electronic Transitions DIET-V*, Eds. A.R. Burns, E.B. Stechel and D.J. Jennison, Vol. 31 of *Springer Series in Surface Science* (Springer, Berlin, 1993) p. 212.
- [33] K.S. Song and R.T. Williams, *Self-trapped Excitons*, Vol. 105 of *Springer Series in Solid-State Sciences*, (Springer, Berlin, 1993).
- [34] R. Bennowitz, C. Günther, M. Reichling, E. Matthias, S. Vijayalakshmi, A.V. Barnes and N.H. Tolk, *Appl. Phys. Lett.* 66 (1995) 320.
- [35] M. Reichling, R. Wiebel, T.A. Green, E. Matthias, in: *Defects in Insulating Materials*, Vol. 2, Eds. O. Kanert and J.-M. Spaeth (World Scientific, Singapore, 1993) p. 1318.
- [36] R. Bennowitz, C. Günther, M. Reichling, E. Matthias, R.M. Wilson and R.T. Williams, *Radiat. Eff. Defects Solids* 137 (1995) 1245.
- [37] R.M. Overney, H. Haefke, E. Meyer and H.-J. Güntherodt, *Surf. Sci.* 277 (1992) L29.
- [38] C.L. Strecker, W.E. Moddeman and J.T. Grant, *J. Appl. Phys.* 52 (1981) 6921.
- [39] K. Saiki, Y. Sato and A. Koma, *Phys. Scr. T* 41 (1992) 255.
- [40] U. Jain and A.B. Lidiard, *Philos. Mag.* 35 (1977) 245.
- [41] M. Reichling, *Nucl. Instrum. Methods B* 101 (1995) 108.
- [42] R. Bennowitz, D. Smith, M. Reichling, E. Matthias, N. Itoh and R.M. Wilson, *Nucl. Instrum. Methods B* 101 (1995) 118.
- [43] B.M.U. Scherzer, in: *Sputtering by Particle Bombardment II*, Topics in Applied Physics, Vol. 52, Ed. R. Behrisch (Springer, Berlin, 1983) p. 271.
- [44] A. van den Bosch, *J. Phys. Chem. Solids* 25 (1964) 1293.
- [45] A. van den Bosch, *Radiat. Eff.* 19 (1973) 129.